CHEMISTRY OF MATERIALS
Article

Chem. Mater. **2009,** *21,* 5485–5490 5485
DOI:10.1021/cm902406e

Mn-Substituted $[Zn_{1-x}Mn_xSe](DETA)_{0.5}$ ($x = 0-0.3$) Inorganic−Organic Hybrid Nanobelts: Synthesis, Electron Paramagnetic Resonance Spectroscopy, and Their Temperature- and Pressure-Dependent Optical Properties

Meng Zhang, Ce Shi, Tie-Kai Zhang, Mei Feng, Ling Chang, Wei-Tang Yao, and Shu-Hong Yu*

Division of Nanomaterials and Chemistry, Hefei National Laboratory for Physical Sciences at Microscale, Department of Chemistry, Department of Materials Science and Engineering, University of Science and Technology of China, Hefei 230026, P. R. China

Received August 5, 2009. Revised Manuscript Received October 13, 2009

Mn-substituted 1D $[Zn_{1-x}Mn_xSe](DETA)_{0.5}$(DETA = diethylenetriamine, $x = 0-0.3$) inorganic−organic hybrid nanobelts have been synthesized by a solvothermal reaction in a mixed solvent media. Strong Mn^{2+} internal transition ($^4T_1 \rightarrow {}^6A_1$) emission peaks at 585 nm (2.12 eV) are detected at room temperature photoluminescence (PL) spectra, and the highest emission intensity is obtained when the nominal Mn content $x = 0.15$. Temperature- and pressure-dependent photoluminescent properties as well as the electron paramagnetic resonance (EPR) spectra of $[Zn_{1-x}Mn_xSe](DETA)_{0.5}$ nanobelts have been studied for the first time. Temperature-dependent PL spectra show that the lower the temperature, the higher the intensity of the emission intensity. Under high pressure, a large red shift of Mn^{2+}-related orange luminescence is observed and luminescent intensity is greatly decreased as the pressure increases to 10.5 GPa. Pressure dependence of the Mn^{2+} PL integrated intensity and energy have the same kink point at 2.54 GPa, which give birth to two PL pressure coefficients in different pressure range.

1. Introduction

Currently, inorganic−organic hybrid nanocomposite materials have attracted significant attention due to their interesting and novel properties which are not easily attainable in either inorganic or organic materials alone.[1,2] Among them, II−VI-based hybrid semiconductors, $MQ(L)_n$ (M = Zn, Cd, Mn; Q = S, Se, Te; L = monoamine, hydrazine, diamine, diethylenetriamine, cyclohexylamine, *m*-xylylenediamine; $n = 0.5$ or 1), a new family of multifunctional hybrid materials, has been synthesized recently,[3] in which subnanometer sized MQ inorganic segments (e.g., slab or chain) are separated by organic spacers L in one structure via coordinate or covalent bonds, and then result in a long-range order periodic structure, like the superlattices or quantum wells.[1,3a] In contrast to nonhybrid semiconductor nanomaterials, for example, quantum dots, these compounds exhibit larger blue shift in their optical absorption edges which means a broader band gap tunability and a higher band-edge absorption simultaneously owing to the quantum confinement effect.[3d,e] Moreover, the physical properties of the hybrid system are conveniently tuned by changing the length of organic amine, the number of inorganic layer and also the anion.[1,3d,e] Besides this, this unique family of II−VI-based hybrid semiconductors exhibit nearly zero uniaxial thermal expansion (ZTE) in a broad temperature range when selecting suitable amine, in virtue of contradiction between positive thermal expansion (PTE) behavior of inorganic semiconductor and negative thermal expansion (NTE) of amine, for example, α- or β-$ZnTe(L)_{0.5}$.[4] It is worth mentioning that the combination of the strongpoint of both PTE materials and organic components would show not only superior electronic and optical properties but also flexibility and lightweight.

At the same time, transition metal doping has also been used as an effective avenue to modulate the properties of inorganic−organic hybrid nanocomposite materials due

*To whom correspondence should be addressed. Fax: + 86 551 3603040. E-mail: shyu@ustc.edu.cn.

(1) Alberti, G.; Costantino, U. In *Comprehensive Supramolecular Chemistry*; Elsevier Science: New York, 1996; Vol. 7, Chapter 1, pp 1−24.
(2) Zhang, Y.; Dalppian, G. M.; Fluegel, B.; Wei, S.-H.; Mascarenhas, A.; Huang, X. Y.; Li, J.; Wang, L. W. *Phys. Rev. Lett.* **2006**, *96*, 026405.
(3) (a) Huang, X. Y.; Li, J.; Fu, H. *J. Am. Chem. Soc.* **2000**, *122*, 8789. (b) Huang, X. Y.; Heulings, H. R.IV; Le., V.; Li, J. *Chem. Mater.* **2001**, *13*, 3754. (c) Deng, Z. X.; Li, L.; Li, Y. D. *Inorg. Chem.* **2003**, *42*, 2331. (d) Huang, X. Y.; Li, J.; Zhang, Y.; Mascarenhas, A. *J. Am. Chem. Soc.* **2003**, *125*, 7049. (e) Huang, X. Y.; Li, J. *J. Am. Chem. Soc.* **2007**, *129*, 3157. (f) Yao, W. T.; Yu, S. H.; Huang, X. Y.; Jiang, J.; Zhao, L. Q.; Pan, L.; Li, J. *Adv. Mater.* **2005**, *17*, 2799. (g) Fan, L. B.; Song, H. W.; Zhao, H. F.; Pan, G. H.; Yu, H. Q.; Bai, X.; Li, S. W.; Lei, Y. Q.; Dai, Q. L.; Qin, R. F.; Wang, T.; Dong, B.; Zheng, Z. H.; Ren, X. G. *J. Phys. Chem. B* **2006**, *110*, 12948. (h) Gawel, B.; Lasocha, W.; Zieba, M. *J. Alloys Compd.* **2007**, *442*, 77.
(4) (a) Zhang, Y.; Islam, Z.; Ren, Y.; Parilla, P. A.; Ahrenkiel, S. P.; Lee, P. L.; Mascarenhas, A.; Mcnevin, M. J.; Fu, H. X.; Huang, X. Y.; Li, J. *Phys. Rev. Lett.* **2007**, *99*, 215901. (b) Li, J.; Bi, W. H.; Ki, W.; Huang, X. Y.; Reddy, S. *J. Am. Chem. Soc.* **2007**, *129*, 14140.

© 2009 American Chemical Society
Published on Web 10/27/2009

to the confinement of the electron and hole together with host-sp and dopant-d hybridization.[5] The improvement of these properties is critical to material applications in optoelectronic devices, information storage, solid-state lighting, and spintronic materials. Until now, many efforts have been spent on synthesis of transition metal-doped $MQ(L)_n$-based hybrid crystals. These works have proved that doping is feasible in this hybrid system to tailor its magnetic[6] or photoluminescent properties[7] and still approximatively hold the structure and band-edge absorption of the hosts. An interesting example is that Mn-doped 2D-[Cd_2S_2(ba)] (ba = *n*-butylamine) with *n*-butylamine as a spacer can give rise to a broad (white-light) emission covering the entire visible spectrum like CdSe nanocrystals[8] caused by their high surface-to-volume ratio, which enables it promising for use in white-light light-emitting diodes (LEDs).[9]

The temperature- and pressure-dependent photoluminescence are predominant test techniques for optical properties and are frequently used to investigate the properties of the luminescent centers in semiconductors. Since the change of temperature can influence the crystal fields surrounding luminescent centers and electron−phonon coupling, resulting in different temperature behavior in different luminescence centers.[10] High pressure photoluminescence (PL) spectra are a popular way to study the electronic structures and phase transition of semiconductor materials related to their structural stability. Under the application of pressure, the interatomic distance and the overlap among adjacent electronic orbits will undergo change, so the pressure dependence of luminescence can provide useful information about the electronic states of the emitters and the interactions between the luminescent centers and their hosts.[11] Temperature- and pressure-dependent photoluminescence have been intensively used to investigate semiconductor nanomaterials or bulk materials; however, it is rarely reported to investigate the inorganic−organic hybrids by this technique, which is of great value to study the structures of the hybrids, consequently the influences of the luminescent centers by the organic component, which would change at a low temperature or high pressure environment. Due to the fact that 1D structures are important building blocks in fabricating electronic, optoelectronic, electrochemical, and electromechanical devices with nanoscale dimensions,[12] recently, we have synthesized uniform [ZnSe](DETA)$_{0.5}$ (DETA = diethylenetriamine) one-dimensional nanobelts in a ternary solution.[3f]

In this paper, we extend this synthesis method for controlled synthesis of Mn-doped [ZnSe](DETA)$_{0.5}$ nanobelts in a mixed solvent system. Temperature- and pressure-dependent photoluminescence as well as the electron paramagnetic resonance (EPR) spectrum of [$Zn_{1-x}Mn_xSe$](DETA)$_{0.5}$ nanobelts have been studied for the first time.

2. Experimental Section

2.1. Synthesis [$Zn_{1-x}Mn_xSe$](DETA)$_{0.5}$ Nanobelts. All reagents are of analytical grade and used without further purification. [$Zn_{1-x}Mn_xSe$](DETA)$_{0.5}$ nanobelts were prepared following our previously reported method with minor modification.[3f] Na_2SeO_3 (0.3 mmol) and 0.3 (1 − *x*) (*x* = 0, 0.05, 0.10, 0.15, 0.20, 0.25, 0.30) mmol of $ZnSO_4 \cdot 7H_2O$ were added into a mixed solution containing 5 mL of hydrazine hydrate, 14 mL of diethylenetriamine, 20*x* mL of 0.015 M $MnSO_4 \cdot H_2O$ solution, and (16−20*x*) mL of deionized water under stirring. The mixed solution was then transferred into a Teflon-lined autoclave (with a filling ratio of 80% v/v). The autoclave was closed and kept at 180 °C for 4 days and, then, cooled to room temperature naturally. The final product was centrifuged and washed several times with double distilled water and absolute ethanol and dried in vacuum at 60 °C for several hours.

2.2. Characterization. The final products were analyzed by X-ray powder diffraction (XRD), scanning electron microscopy (SEM), transmission electron microscopy (TEM), energy-dispersive spectrometry (EDS), inductively coupled plasma-atomic emission spectra (ICP-AES), electron paramagnetic resonance (EPR), UV−vis, and photoluminescence (PL), respectively. XRD analyses were carried on a Philips X'Pert PRO SUPER X-ray diffractometer equipped with graphite monochromatized Cu Kα radiation (λ = 1.54056 Å), and the operation voltage and current were maintained at 40 kV and 40 mA, respectively. Before XRD analyses, the powders had been grinded adequately. The morphology was examined with a JEOL JSM-6700F SEM, and TEM was performed on a Hitachi (Tokyo, Japan) H-800 transmission electron microscope at an accelerating voltage of 200 kV. The percentages of Mn present in the final samples were estimated by ICP-AES using an Atomscan Advantage spectrometer, Therma Jarrell Ash Corp. Room temperature EPR spectra were performed on JEOL JES-FA200 EPR spectrometer (300 K, 9064 MHz, X-band), and UV−vis absorption spectra were obtained using a UV-2550 spectrometer (Shimadzu). The samples had been predispersed well in ethanol by ultrasonic treatment. The room temperature and low temperature PL spectra were performed at the Time-Resolved Spectroscopy Station of the National Synchrotron Radiation Laboratory (NSRL, Hefei, China). All the room-temperature

(5) (a) Norris, D. J.; Yao, N.; Charnock, F. T.; Kennedy, T. A. *Nano Lett*. **2001**, *1*, 3. (b) Radovanovic, P. V.; Norberg, N. S.; Mcnally, K. E.; Gamelin, D. R. *J. Am. Chem. Soc*. **2002**, *124*, 15192.
(6) (a) Heulings, H. R.IV; Huang, X. Y.; Li, J. *Nano Lett*. **2001**, *1*, 521. (b) Huang, X. Y.; Heulings, H. R.IV; Li, J.; Yuen, T.; Lin, C. L. *J. Nanosci. Nanotechnol*. **2005**, *5*, 1.
(7) (a) Lu, J.; Wei, S.; Peng, Y. Y.; Yu, W. C.; Qian, Y. T. *J. Phys. Chem. B*. **2003**, *107*, 3427. (b) Lu, J.; Wei, S.; Yu, W. C.; Zhang, H. B.; Qian, Y. T. *Chem. Mater*. **2005**, *17*, 1698.
(8) Bowers, M. J.; McBride, J. R.; Rosenthal, S. J. *J. Am. Chem. Soc*. **2005**, *127*, 15378.
(9) Ki, W.; Li, J. *J. Am. Chem. Soc*. **2008**, *130*, 8114.
(10) (a) Xiang, B.; Wang, P. W.; Zhang, X. Z.; Dayeh, S. A.; Aplin, D. P. R.; Soci, C.; Yu, D. P.; Wang, D. L. *Nano Lett*. **2007**, *7*, 323. (b) Mizoguchi, H.; Woodward, P. M.; Park, C. H.; Keszler, D. A. *J. Am. Chem. Soc*. **2004**, *126*, 9796. (c) Mahamuni, S.; Lad, A. D.; Patole, S. *J. Phys. Chem. C* **2008**, *112*, 2271.
(11) (a) Grant, C. D.; Crowhurst, J. C.; Hamel, S.; Williamson, A. J.; Zaitseva, N. *Small* **2008**, *4*, 788. (b) Kim, B. S.; Kuskovsky, L. L.; Herman, C. T. I. P.; Neumark, G. F.; Guo, S. P.; Tamargo, M. C. *App. Phys. Lett*. **2001**, *78*, 4151. (c) Arora, A. K.; Sakuntala, T. *Phys. Rev. B* **1995**, *52*, 11052. (d) Su, F. H.; Fang, Z. L.; Ma, B. S.; Ding, K.; Li, G. H.; Chen, W. J. *J. Phys. Chem. B* **2003**, *107*, 6991. (e) Ni, Z. H.; Fan, H. M.; Kasim, J.; You, Y. M.; Feng, Y. P.; Han, M. Y.; Shen, Z. X. *J. Phys.: Condens. Matter* **2008**, *20*, 325214. (f) Su, F. H.; Fang, Z. L.; Ma, B. S.; Ding, K.; Li, G. H.; Xu, S. J. *J. Appl. Phys*. **2004**, *95*, 3344.
(12) Xia, Y. D.; Yang, P. D.; Sun, Y. G.; Wu, Y. Y.; Mayers, B.; Gates, B.; Yin, Y. D.; Kim, F.; Yan, Y. Q. *Adv. Mater*. **2003**, *15*, 353.

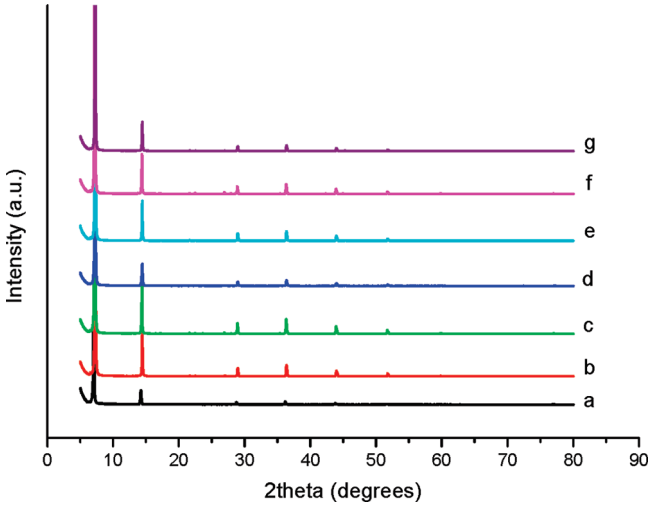

Figure 1. Powder X-ray diffraction patterns of synthesized [ZnSe](DETA)$_{0.5}$ and [Zn$_{1-x}$Mn$_x$Se](DETA)$_{0.5}$ nanobelts with different Mn contents. Patterns from (a) to (g) correspond to the nominal Mn content x = 0, 0.05, 0.10, 0.15, 0.20, 0.25, and 0.30, respectively.

PL spectra were measured under the same conditions, for example, the same mass of powder samples and the same excitation light intensity. The PL measurements under pressure were done in a gasketed diamond-anvil cell (DAC) at room temperature. Some powders of the samples, together with a piece of ruby chip, were placed in a stainless-steel gasket with a hole of 160 μm in diameter. The pressure was determined by the use of the standard ruby fluorescence technique.

3. Results and Discussion

3.1. Preparation and Characterization of [Zn$_{1-x}$Mn$_x$Se](DETA)$_{0.5}$ Nanobelts. Figure 1 shows powder X-ray diffraction (PXRD) patterns of the products, with the nominal Mn content x = 0.05, 0.10, 0.15, 0.20, 0.25, and 0.30. As is known before, the sample with x = 0 can be indexed as [ZnSe](DETA)$_{0.5}$ with an orthorhombic phase $Cmc2_1$. No impurity peaks (for example, MnSe) are detected when Mn is introduced, which indicates the probable uniform doping throughout the samples. The samples were further analyzed by component analysis and EPR. The schematic structure illustrations are shown in Figure 2, which were reported previously.[3f] All molecular simulations were carried out with software package: Materials Studio, Version 4.1, Accelrys Inc., San Diego, CA (USA), 2008.

3.2. Morphology of [Zn$_{1-x}$Mn$_x$Se](DETA)$_{0.5}$ Nanobelts. Figure 3a shows that [Zn$_{1-x}$Mn$_x$Se](DETA)$_{0.5}$ nanobelts (the nominal Mn content x is 0.15) have lengths in the range of 10−20 μm and their average thickness is of about 40 nm. The belts have a smooth surface and are flexile. TEM observation in Figure 4 shows that the doped belts have a width of 200−400 nm. The results indicated that the Mn doping will not change its beltlike shape even when the nominal Mn content x reaches 0.30. However, when the nominal Mn content x is more than or equal to 0.20, a sort of irregular particles appears besides the belts (see Figure S1 in the Supporting Information) and the particles manifold with a further increase in the nominal Mn doping content x. Because there is no additional diffraction peaks identified even in partly enlarged XRD patterns (see Figure S2 in the Supporting Information), HRTEM and EDS are used to characterize these irregular particles. A HRTEM image taken from the edge of a grain (see Figure S3a,b in the Supporting Information), showing lattice spacings of ca 3.51 and 3.52 Å, respectively, corresponding to the lattice spacings of the (100) planes and (010) planes for wurtzite ZnSe, respectively. The angle of the planes of (100) and (010) is 110°, which is consistent with that calculated result according to its crystal structure. Energy dispersive X-ray spectrum (EDX) analysis performed on different selected areas of the grains shows that the elements are Zn, Mn, and Se with a mean molar ratio of 54.0:2.3:43.7 (see Figure S4 in the Supporting Information).

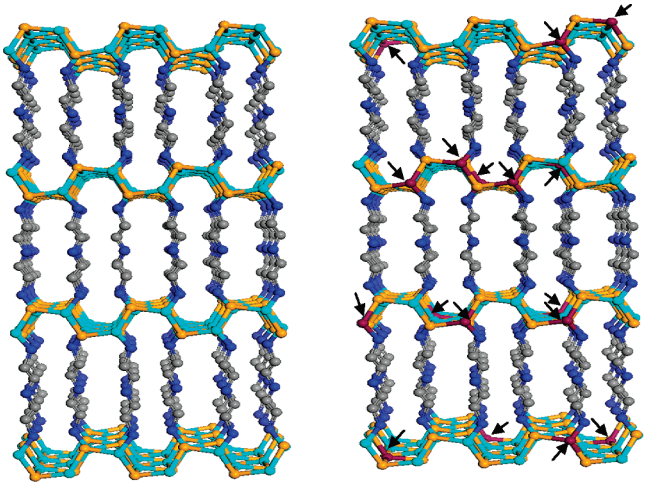

Figure 2. Schematic illustrations of the crystal structures of [ZnSe](DETA)$_{0.5}$ and [Zn$_{1-x}$Mn$_x$Se](DETA)$_{0.5}$ nanobelts. The light-blue cylinders are Zn, the saffron cylinders represent Se, and the blue and gray cylinders are N and C, respectively. The introduced Mn are shown with brown cylinders and marked with arrows.

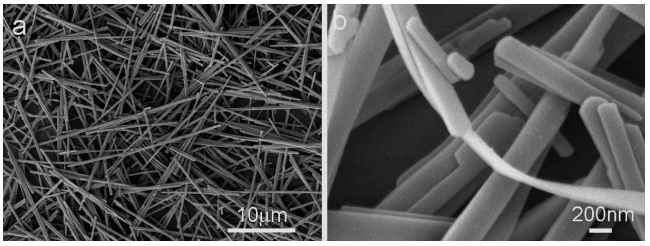

Figure 3. SEM images of [Zn$_{0.85}$Mn$_{0.15}$Se](DETA)$_{0.5}$ nanobelts.

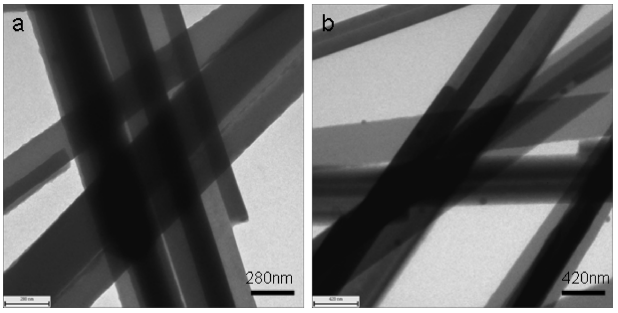

Figure 4. TEM images of [Zn$_{0.85}$Mn$_{0.15}$Se](DETA)$_{0.5}$ nanobelts.

Table 1. Nominal Mn Content in the Reaction Mixture and the Experimental Mn Composition As Determined by ICP-AES Analysis

Mn % nominal	5	10	15	20	30
Mn % ICP-AES	0.14	0.20	1.30	8.21	11.96

Thus, it can be assumed that these structure features are due to the presence of inorganic phase $Zn_{1-x}Mn_xSe$ in the sample.

3.3. Mn Content in $[Zn_{1-x}Mn_xSe](DETA)_{0.5}$ Nanobelts. ICP-AES are used to determine the Mn content as shown in Table 1. It is seen that the amount of Mn incorporated into the $[ZnSe](DETA)_{0.5}$ nanobelts is little, but when the nominal content x is more than or equal to 0.20, the amounts of incorporated Mn have a distinct increase, concurring with the appearance of irregular $Zn_{1-x}Mn_xSe$ grains (see Figure S1 in the Supporting Information). Thus, excessive doping in inorganic−organic hybrid semiconductors is more inclined to form inorganic diluted magnetic semiconductors (DMSs), which means that doping in inorganic−organic hybrid semiconductors could be compared with nonhybrid ones.

3.4. EPR Spectroscopy of $[Zn_{1-x}Mn_xSe](DETA)_{0.5}$ Nanobelts. Electron paramagnetic resonance (EPR) as an accurate probe is used to study the Mn^{2+} coordination state, and $Mn^{2+}-Mn^{2+}$ interaction for Mn^{2+} ($S = 5/2$) is sensitive to its coordination environment (Figure 5). There are a series of hyperfine lines in the spectrum (a) (the nominal Mn content $x = 0.05$) which can be identified as two signals. With the increase of Mn content, one signal (signal 1) intensifies while the other (signal 2) disappears as shown in the spectrum (b). For signal 1, a hyperfine splitting of $A = 61.98 \times 10^{-4}$ cm^{-1} can be extracted, which agrees well with that obtained from substitutional doping Mn^{2+} in ZnSe crystal (61.7×10^{-4} cm^{-1}),[10c,13] indicating Mn is substitutionally incorporated into the host lattice. Signal 2, whose hyperfine splitting A is about 57.8×10^{-4} cm^{-1}, disappears when the nominal Mn content increases to $x = 0.10$. So the signal 2 is not given by Mn^{2+} ions located near the surface, or else the signal would not become weakened with increasing the doping content, and the signal caused by Mn^{2+} ions at the surface should have exhibited a larger hyperfine splitting due to its strong ionic activity.[14] Thus, we can conclude that signal 2 comes of forbidden transition ($\Delta m_S = \pm 1, \Delta m_I = \pm 1$).[12d,15] When the nominal Mn content reaches up to $x = 0.15$, a broadband shows up and the six hyperfine lines almost disappear, which indicates that $Mn^{2+}-Mn^{2+}$ interaction has been dominant and only few isolated Mn^{2+} ions still exist.

3.5. Photoluminescence Property of $[Zn_{1-x}Mn_xSe](DETA)_{0.5}$ Nanobelts. Figure 6 shows the room-temperature PL spectra with 300 nm excitation, indicating a

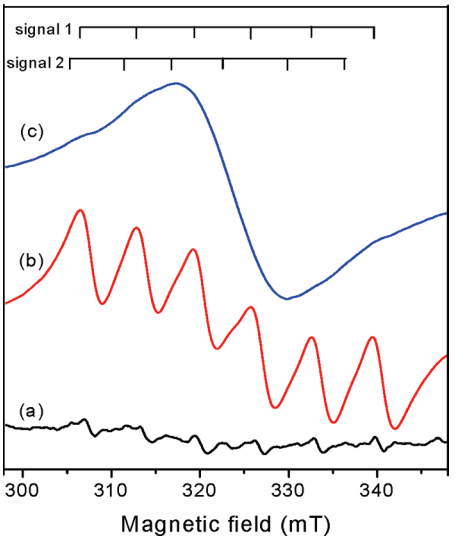

Figure 5. Electron paramagnetic resonance (EPR) spectra of $[Zn_{1-x}Mn_xSe](DETA)_{0.5}$ nanobelts with different Mn^{2+} nominal contents: (a) $x = 0.05$; (b) $x = 0.10$; (c) $x = 0.15$.

distinct emission band centered at 585 nm for all the products, originating from Mn^{2+} internal d−d ($^4T_1 \rightarrow {}^6A_1$) transition which consists of bulk and nanocrystals $Zn_{1-x}Mn_xSe$ DMS[11a,16] (the band centered at 600 nm is the double frequency peak of the 300 nm excitation). This is another piece of evidence in favor of successful doping besides EPR data. All the room-temperature PL spectra were measured under the same conditions for comparison. With the increase of nominal Mn content, the emission peaks at 585 nm will not shift but intensities will first increase from the nominal Mn content $x = 0$ to $x = 0.15$ and then decrease when the nominal Mn content $x > 0.15$, as shown in the inset of Figure 6. There will be more effective substitution of Mn^{2+} ions at the tetrahedral coordinate sites contributing to the Mn^{2+}-related emission while increasing doping content. Excessive doping ($x > 0.15$) will enhance $Mn^{2+}-Mn^{2+}$ interaction due to their close proximity as well as the formation of inorganic $Zn_{1-x}Mn_xSe$ which would answer for the Mn^{2+} luminescence quench.[17] Thus, an appropriate doping amount is vital to achieve the maximal photoluminescence intensity. Obviously, in the present experiments, the maximal intensity appears at the nominal Mn doping content $x = 0.15$ which corresponds to 0.013 of the exact doping amount determined by ICP-AES. Band-edge absorption peaks at about 310 nm (4.00 eV) are observed and almost have no shift complying with altered Mn content (see Figure S4 in the Supporting Information). Besides this, two minor peaks appeared at 266 nm (4.66 eV) and 286 nm (4.34 eV) whose origins have not been not entirely clear up to now.[3f] Compared with our previous results,[3f] all of the three peaks have a red shift from 260, 284, and 295 nm, respectively. Prolonging the reaction time will destroy inorganic−organic hybrid structure and only pure inorganic

(13) (a) Ludwig, G. W.; Woodbury, H. H. Electron Spin Resonance in Semiconductors. In *Solid State Physics*; Seitz, F., Turnbull, D., Eds.; Academic Press: New York, 1962; Vol. *13*, p 298. (b) Norris, D. J.; Yao, N.; Charnock, F. T.; Kennedy, T. A. *Nano Lett.* **2001**, *1*, 3.
(14) Magana, D.; Perera, S. C.; Harter, A. G.; Dalai, N. S.; Strouse, G. F. *J. Am. Chem. Soc.* **2006**, *128*, 2931.
(15) Gonzalez Beermann, P. A.; McGarvey, B. R.; Muralidharan, S.; Sung, R. C. W. *Chem. Mater.* **2004**, *16*, 915.
(16) Waldmann, H.; Benecke, C.; Busse, W.; Gumlich, H.-E.; Krost, A. *Semicond. Sci. Technol.* **1989**, *4*, 71.
(17) Borse, P. H.; Srinivas, D.; Shinde, R. F.; Date, S. K.; Vogel, W.; Kulkarni, S. K. *Phys. Rev. B* **1999**, *60*, 8659.

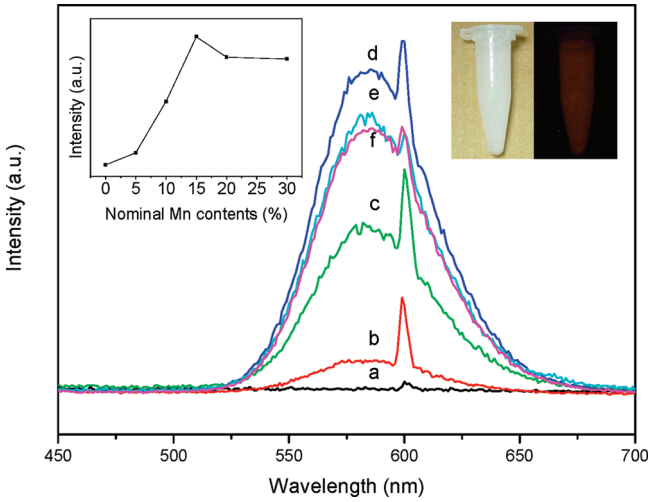

Figure 6. Room-temperature photoluminescence (PL) spectra of synthesized $[ZnSe](DETA)_{0.5}$ and $[Zn_{1-x}Mn_xSe](DETA)_{0.5}$ nanobelts with different Mn contents. The excitation wavelength is 300 nm (4.13 eV). Curves from (a) to (f) correspond to the nominal Mn content $x = 0$, 0.05, 0.10, 0.15, 0.20, and 0.30, respectively. Inset (left) shows the pattern of the PL integrated intensity versus Mn contents and inset (right) shows the color of the sample before and after illumination at $\lambda = 365$ nm.

semiconductor can be obtained. In the present experiments, prolonging the reaction time for the sake of successful doping may do harm to hybrid structures to some extent, which would reduce quantum confinement effect answering for the red shift of absorption peaks.

3.6. Temperature- and Pressure-Dependent Photoluminescence of $[Zn_{1-x}Mn_xSe](DETA)_{0.5}$ Nanobelts. The temperature- and pressure-dependent photoluminescence techniques are frequently used to investigate the properties of the luminescence centers in inorganic semiconductors. However, the technique applied for investigation of the inorganic−organic hybrid system has rarely been reported[18] and still needs to open out. PL spectra are studied at temperatures ranging from 255 to 30 K as shown in Figure 7 with the nominal Mn content $x = 0.15$ as an example.

Mn^{2+}-related orange luminescence at 585 nm still exists, and intensity is greatly enhanced as the temperature decreases to 30 K, as shown in the inset of Figure 7 (the peak at around 596 nm is the double frequency peak of the 298 nm excitation). Similar effects are observed in the case of the nominal Mn content $x = 0.10$ and $x = 0.20$ (data not shown). The same phenomena have been seen in other nonhybrid materials, such as $Zn_{1-x}Mn_xSe$ DMSs, indicating the effective substitution of the Mn^{2+} ions at the tetrahedral coordinates.[19] However, the red shift illustrated in their $Zn_{1-x}Mn_xSe$ DMSs associated with d−d exchange interactions, which lowers the energy for the transition from the excited to the ground state, is not obviously observed here. There are no antiferromagnetic d−d interactions between Mn^{2+} ions here, which are caused by the very low concentrations of Mn^{2+} in lattices

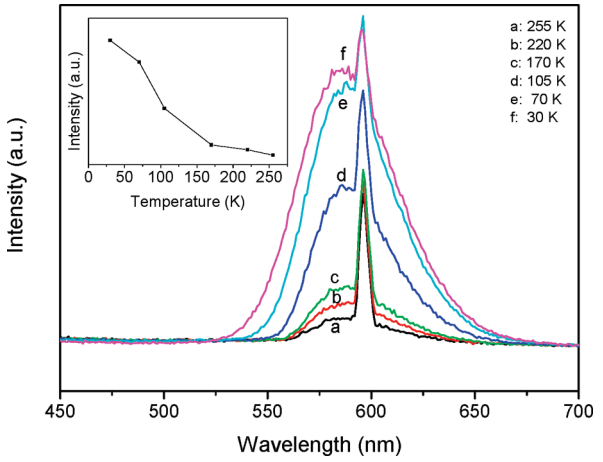

Figure 7. Temperature-dependent PL spectra for $[Zn_{0.85}Mn_{0.15}Se](DETA)_{0.5}$ nanobelts. The excitation wavelength is 298 nm (4.16 eV). Curves from (a) to (f) correspond to $T = 225$, 220, 170, 105, 70, and 30 K, respectively. Inset pattern shows the pattern of the PL integrated intensity versus temperature.

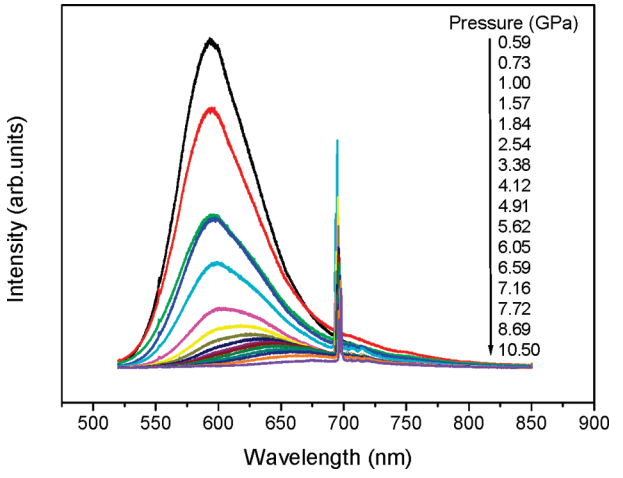

Figure 8. Pressure-dependent PL spectra for $[Zn_{0.85}Mn_{0.15}Se](DETA)_{0.5}$ nanobelts. The excitation wavelength is 514.5 nm (2.41 eV).

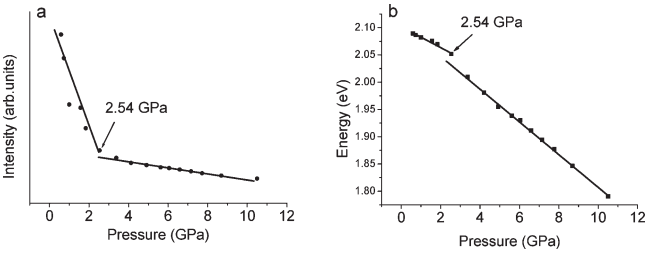

Figure 9. Pressure dependence of the Mn^{2+} PL integrated intensity (a) and energy (b) for $[Zn_{0.85}Mn_{0.15}Se](DETA)_{0.5}$ nanobelts.

to impact the crystal field between the $^4T_1$ and $^6A_1$ states, perhaps responsible for this undiscovered shift.[20]

Next, we have studied PL spectra of $[Zn_{1-x}Mn_xSe](DETA)_{0.5}$ nanobelts under pressure. Figure 8 depicts the PL spectra of $[Zn_{0.85}Mn_{0.15}Se](DETA)_{0.5}$ nanobelts measured at room temperature with increasing pressure. A large red shift of Mn^{2+}-related orange luminescence

(18) Matsuishi, K.; Ishihara, T.; Onari, S.; Chang, Y. H.; Park, C. H. *Phys. Status Solidi B* **2004**, *241*, 3328.
(19) (a) MacKay, J. F.; Becker, W. M.; Spaek, J.; Debska, U. *Phys. Rev. B* **1990**, *42*, 1743. (b) Lee, J. Y.; Kim, D. S.; Kang, J. H.; Yoon, S. W.; Lee, H.; Park, J. *J. Phys. Chem. B* **2006**, *110*, 25869.
(20) Xue, J.; Ye, Y.; Medina, F.; Martinez, L.; Lopez-Rivera, S. A.; Giriat, W. *J. Lumin.* **1998**, *78*, 173.

is observed, and luminescence intensity is greatly decreased as the pressure increases to 10.5 GPa, which can be seen more clearly in Figure 9 (the peak at around 696 nm is the standard ruby fluorescence used to determine the pressure). From Figure 9a, we can also see that the PL integrated intensity decreases rapidly with increasing pressure up to about 2.54 GPa and then decreases slowly. The PL energy as a function of pressure is shown in Figure 9b. The data can be fitted with the following formula:

$$E(P) = E_0 + \alpha P$$

Where E_0 is the ambient pressure PL energy, α is the PL pressure coefficient, and P is the applied pressure. It is found that, at lower pressure, the PL energy of $[Zn_{0.85}Mn_{0.15}Se](DETA)_{0.5}$ nanobelts shifts linearly with a pressure coefficient of -19 meV/GPa. Above 2.54 GPa, the PL peak also shifts linearly with pressure but the pressure coefficient changes to -30 meV/GPa. As for pressure coefficient $\alpha = -30$ meV/GPa, it is in excellent agreement with that of calculated pressure coefficient of the Mn^{2+}-orange emission using the crystal field theory,[11f] which indicates a phase transition trend from direct to indirect gap semiconductors.[11c] The other pressure coefficient at lower pressure, to our best knowledge, has not been reported for ZnSe-based inorganic compounds so far. Considering organic diethylenetriamine is "limper" compared with inorganic ZnSe and then is easy to be compressed, we propose that this PL peak also shifted linearly with the pressure coefficient due to the compression effect of diethylenetriamine molecules. It is interesting to note that pressure dependence of PL integrated intensity and PL energy have the same kink point at 2.54 GPa, which means the same mechanism between them. We can also attribute the rapid decreases of PL integrated intensity before 2.54 GPa to the compression effect of diethylenetriamine molecules. This is consistent with a previous study that Mn^{2+}-related orange emission intensities increase monotonically with the length of the organic monoamines.[7,8] Compression of diethylenetriamine (DETA) molecules in $[Zn_{1-x}Mn_xSe](DETA)_{0.5}$ under pressure makes the interlayer manganese interactions enhanced due to their close proximity and then decreases the emission intensities. Another remarkable feature is that the decreases of PL intensity are reversible. When pressure is released, the PL can resume immediately (see Figure S6 in the Supporting Information). Because this process is irreversible for pure inorganic ZnSe nanomaterials,[11c] the only reasonable interpretation here is that diethylenetriamine was elastic and recovered upon release of pressure. This further confirmed that decreases of Mn^{2+} PL integrated intensity and red shift of the Mn^{2+}-related orange emission band is due to the compression effect of diethylenetriamine molecules within the $[Zn_{1-x}Mn_xSe](DETA)_{0.5}$ structure.

4. Conclusions

In summary, $[Zn_{1-x}Mn_xSe](DETA)_{0.5}$ nanobelts have been synthesized by a solvothermal reaction and their temperature and pressure behaviors have been investigated systematically. A strong Mn^{2+}-related orange emission band at 585 nm is observed for the $[Zn_xMn_{0.15}Se](DETA)_{0.5}$ nanobelts at room temperature. The maximum emission intensities can be obtained in the case of nominal Mn content $x = 0.15$. For nominal Mn content $x = 0.15$, the intensity of Mn^{2+}-related orange luminescence at 585 nm is greatly enhanced as the temperature decreased to 30 K without shifting in peak positions. Under pressure, a large red shift of Mn^{2+}-related orange luminescence was observed and luminescence intensity was greatly decreased as the pressure increased to 10.5 GPa. Being a kink point at 2.54 GPa, the PL energy varies linearly with the pressure separately and presents two pressure coefficients. The pressure coefficient at high pressure should be due to a phase transition trend from direct to indirect gap semiconductors, while the one at low pressure is deduced to be due to a compression effect of diethylenetriamine molecules. The EPR spectra of $[Zn_{1-x}Mn_xSe](DETA)_{0.5}$ nanobelts have been studied. These new observations may be helpful for further understanding the photoluminescent mechanisms in doped inorganic−organic hybrid semiconducting nanostructures.

Acknowledgment. S.-H.Y. acknowledges the special funding support from the National Basic Research Program of China (2010CB934700), the National Natural Science Foundation of China (NSFC, Nos. 50732006, 20671085, and 20701035), and the Partner-Group of the Chinese Academy of Sciences-the Max Planck Society. M.Z. thanks National Synchrotron Radiation Laboratory (Hefei, China) for granting Innovation Foundation of NSRL for a graduate student. We thank the help with PL measurement at high pressure from Professor Zejun Ding and Dr. Rucheng Dai in Department of Physics, University of Science and Technology of China.

Supporting Information Available: Figures S1−S6 are available as Supporting Information (PDF). This material is available free of charge via the Internet at http://pubs.acs.org.